Rodríguez-Rodríguez, H.; De Lorenzo, S.; De La Cueva, L.; Salas, G.; Arias-Gonzalez, JR. (2018). Optical Trapping of Single Nanostructures in a Weakly Focused Beam. Application to Magnetic Nanoparticles. The Journal of Physical Chemistry C. 122(31):18094-18101. https://doi.org/10.1021/acs.jpcc.8b04676

Optical Trapping of Single Nanostructures in a Weakly-Focused Beam. Application to Magnetic Nanoparticles

Héctor Rodríguez-Rodríguez,[†,‡] Sara de Lorenzo,[†] Leonor de la Cueva,[†] Gorka Salas,[†,¶] and J. Ricardo Arias-Gonzalez[*,†,¶]

†*Instituto Madrileño de Estudios Avanzados en Nanociencia, C/Faraday 9, Cantoblanco, 28049 Madrid, Spain*

‡*Departamento de Química-Física Aplicada, Universidad Autónoma de Madrid, Cantoblanco, 28049, Madrid, Spain*

¶*CNB-CSIC-IMDEA Nanociencia Associated Unit "Unidad de Nanobiotecnología"*

E-mail: ricardo.arias@imdea.org

Abstract

Optical trapping of individual particles is believed to be only effective under highly-focused beams because these conditions strengthen the gradient forces. This is especially critical in the beam propagating direction, where the scattering and absorption forces must be counterbalanced. Here, we demonstrate that optical trapping of nanostructures is also possible in a weakly-focused beam. We study the theoretical conditions for effective three-dimensional optical confinement and verify them experimentally on iron-oxide-based nanoparticles with and without a silica coating, for which scattering, absorption and gradient forces exist. This chemical approach to their all-optical control is, in turn, convenient for making magnetic nanostructures biocompatible. Weakly-focused beams reduce the irradiance in the focal region and therefore the photon damage to the samples, which is further important to delay quantum dot quenching in the trap or to prevent artifacts in the study of biomolecular motor dynamics.

Introduction

Optical trapping is a now mature strategy to both manipulate objects and measure forces by way of light. From a practical viewpoint, it is currently being exploited in the manipulation of small structures, from micro and nanoparticles (NPs) to molecules and atoms, in a wealth of interdisciplinary research topics.[1–7] Its power relies on the fact that control over the trapped specimens is contactless and with pico-Newton forces, which are high enough to overcome thermal effects and low enough to maintain the integrity of the specimens. In many cases, however, the optical concentration of light energy in typical optical tweezers setups, namely, those in which a monochromatic beam is focused to a diffraction-limited spot,[8] may be detrimental. A high-trapping irradiance may affect the dynamics of the trapped specimen, as, for example, in biomolecular processes[9] or artificial engines,[10] accelerate chemical changes, like those taking place in quantum dot luminescence[11] and, ultimately, generate irreversible functional damages to the sample, which may happen during intracellular manipulation.[12]

Efficient single-beam traps are based on a highly-focused monomode laser, which involves a tight confinement. This is desired to decrease the effect of the thermal fluctuations and increase the spatial localization of the sample, all in all optimizing the fine manoeuvrability of the trapped specimen. Optical trapping in highly-focused beams has been studied both theoretically and experimentally to optimize trapping efficiency and force measurements.[13–20] The reduction of optical irradiances in the trap is, however, antagonist to this optical design. Optical traps with weakly-focused beams imply large focal regions and low optical forces hence posing the question as to what extent optical trapping is effective.

From a technical viewpoint, typical objectives in optical tweezers setups are high numerical aperture (NA) lenses (NA$= 1.2 - 1.4$), which produce tight traps. Loose traps can be implemented by using low NAs ($\lesssim 0.5$).[21] Some researchers, however, implement low-numerical aperture beams (NA_b) inside these objectives by beam underfilling of their entrance pupil.[22–24] The technical interests of weakly-focused optical traps generated with high-NA objective lenses are, first, that this methodology makes possible to move the optical trap without strong distortion of the beam by the objective's pupils; second, that it makes possible to collimate and recover all the scattered light after the trap, which is necessary to calibrate the setup as a force sensor by using the light linear momentum conservation principle;[24,25] and third, that low-NA_b beams are less prone to suffer from severe spherical aberration.[26]

In this article, we study theoretically the conditions for effective optical trapping of single NPs under low focusing. We find equilibrium positions of the NP within the broad focal region and stiffness constants in the three spatial directions. In a second part, we test our theoretical results with two types of particles, an Fe_3O_4 NP and a stratified particle composed by an Fe_3O_4 core coated by an SiO_2 shell (Fe_3O_4@SiO_2), both of which exhibiting optical scattering and absorption but differing in their optical stability in the trap. Iron oxide NPs are of strategical importance for nanomedicine and other applications, in particular for magnetic and optical hyperthermia treatment in oncology and imaging.[27–32]

Methods

Nanoparticle sample preparation

We synthesized plain and silica-coated iron oxide NPs with different core and shell sizes, as described in the Supporting Information. Figure 1 shows TEM images and size statistics for the main core and core-shell systems herein used. Figures S1 and S2 in the Supporting Information shows additional preparations therein analyzed and Figure S3, the magnetic characterizations.

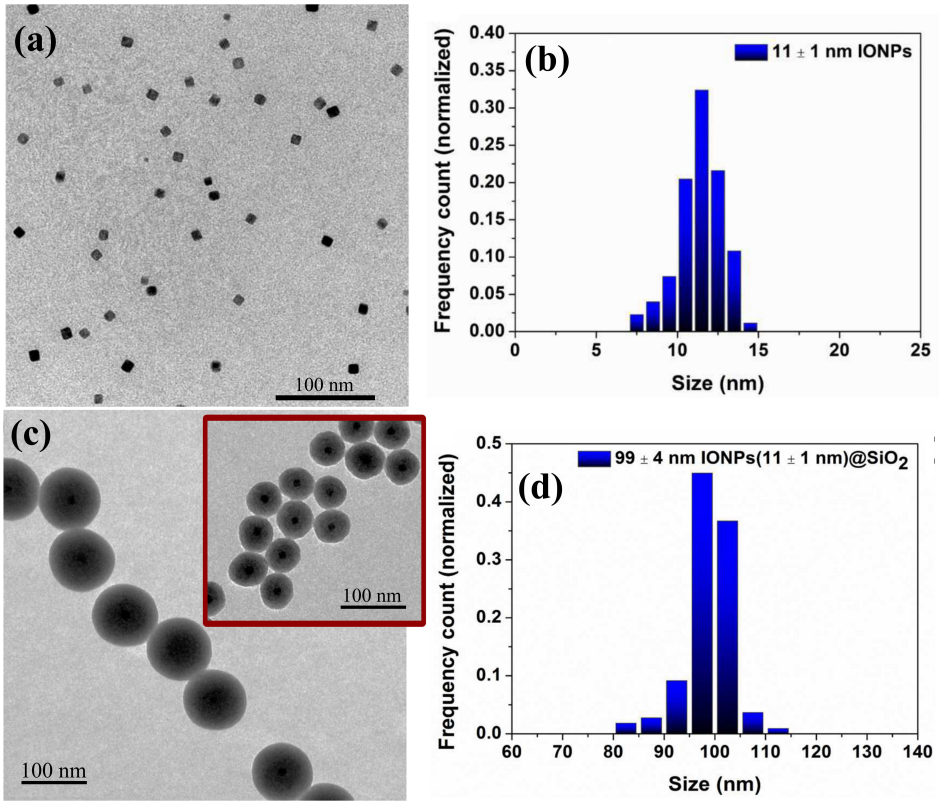

Figure 1: Transmission electron microscopy (TEM) image, (a), and normalized size distribution histogram, (b), of $\varnothing = 11 \pm 1$ nm Fe_3O_4 NPs. These NPs were encapsulated in SiO_2 in a two-step process (Supporting Information). TEM images, (c), and normalized size distribution histogram, (d), of $\varnothing = 99 \pm 4$ nm final Fe_3O_4@SiO_2 NPs. Inset image in (c) corresponds to Fe_3O_4 cores encapsulated with SiO_2 after 24 h of reaction and the main image in this panel to the same preparation after a re-growth reaction of 24 h additional time.

Optical tweezers experimental setup

We used a so called miniTweezers,[33] which is a compact instrument suspended from the ceiling with reduced mechanical drift. The miniaturized configuration also reduces optical path lengths, all in all affording larger measurement stability over time. This apparatus is capable of measuring forces as changes in light-momentum flux. Since this direct measurement of the force is not based on trap stiffness, force calibration is independent of the trapped specimen's size, shape, or refractive index; the viscosity or refractive index of the solution or variations in laser power.[24]

In this instrument, we used a diode laser (250 mW at maximum output power and $\lambda = 808$ nm from Lumics) with circular polarization. The beam is focused by a water-immersion objective, 60X, NA= 1.20 (Olympus, UPLSAPO 60XW) to form the optical trap in a microfluidics chamber. The maximum laser power in the optical trap was 125 mW. The light exiting the trap is collected by a similar objective lens in the forward direction and by the focusing objective lens in the backward direction, and redirected to position-sensitive detectors, which monitor the three force components acting on the trapped particle.

For the calibration based on the conservation of light momentum, it is necessary that all the light exiting the trap is collected; the numerical aperture of the beams is then reduced to approximately $\mathrm{NA}_b = 0.5$, which allows the objective lenses to act as both light focusing elements and collectors.

Stokes' law and power spectrum density measurements

The drag coefficient, γ, of a particle in the trap was determined by moving the microfluidic chamber and recording simultaneously the displacement velocity and the drag force. Then, from Stokes' law, $F_{drag} = \gamma v_{drag}$, it is straightforward to obtain γ as linear fitting. Thermal noise analysis was performed over force fluctuations, Figure 2, acquired at $2^{19} = 524288$ Hz during 10 s for the y-axis and at 600 Hz during approximately 30 s for the z-axis. Data were divided in subintervals for Fourier-transform and subsequent averaging. The corner

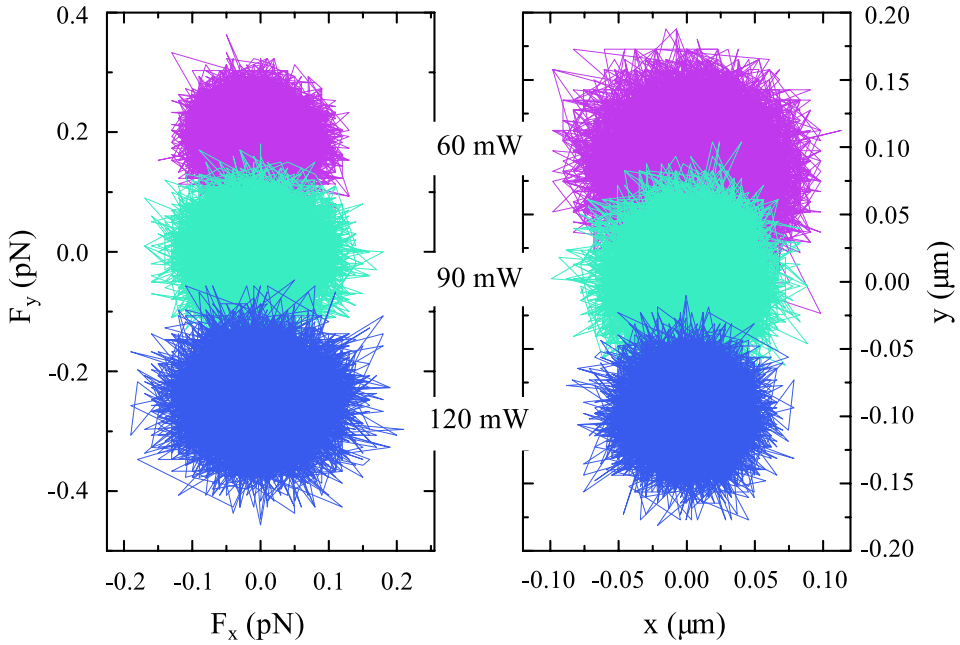

Figure 2: Left panel, force fluctuation of a single optically-trapped Fe_3O_4@SiO_2 (core-shell system shown in Figure 1, (c) and (d)), at three different laser powers. Data were acquired during approximately 30 s at a sampling frequency of 600 Hz. Right panel, corresponding position fluctuations of the same NP calculated by Hooke's law using the experimentally-determined trapping stiffness. Fluctuations are isotropic in the plane perpendicular to the optical axis. In addition, it is observed that while the amplitude of the force fluctuations increases with the optical power in the trap, the amplitude of position fluctuations decreases with power, indicating, as expected, a growing spatial confinement with power.

frequency, f_c, was obtained by fitting to the equilibrium power spectrum density (PSD) of an overdamped particle in a harmonic potential $\langle \Delta F^2(f) \rangle_{eq} = 2\gamma k_B T f_c^2/(f^2 + f_c^2)$, where f is the frequency and $k_B T$ is the thermal energy.

Theory

We model the beam before the focusing element (the objective lens) by a plane wave propagating along the $\hat{z}$ direction. The electric field, $\vec{\mathcal{E}}(\mathbf{r}, t) = \Re e \{\mathbf{E}(\mathbf{r}) \exp(-i\omega t)\}$, can be expressed as a sum of two components, one along the $\hat{x}$ direction and the other along $\hat{y}$, with

the next Jones general polarization state representation:

$$\mathbf{E} = E_x\hat{x} + E_y\hat{y} \sim \frac{1}{\sqrt{|f_x|^2 + |f_y|^2}} \left(f_x\hat{x} + f_y\hat{y}\right), \tag{1}$$

where f_x and f_y are complex numbers that address the amplitude and phase changes that E_x and E_y experience before the focusing of the beam. In particular, wave plates and polarizing beam splitters may be used to combine several beams with similar or equal wavelengths to avoid interference effects in the focal region, which are detrimental for trapping. In some optical tweezers setups, circular polarization in the focal region takes place as a consequence of the use of retarders.[24]

Weakly-focused beam model

After the objective lens, each component is converted into a focused beam thus carrying its respective amplitude and phase difference. If the NA of the combined beam is low enough, the total electric field can be treated by using a paraxial-wave approximation, the Gaussian beam:[34]

$$\mathbf{E}(\mathbf{r}) = \frac{1}{\sqrt{p}} E_0 U(\mathbf{r}) \left(-f_x\hat{x} - f_y\hat{y} + \frac{f_x x + f_y y}{z + iz_0}\hat{z}\right), \tag{2}$$

where $\mathbf{r} = x\hat{x} + y\hat{y} + z\hat{z}$, $p = |f_x|^2 + |f_y|^2$ and E_0 is a complex number addressing global amplitude and phase changes within the objective lens. The complex Gaussian amplitude is:

$$U(\mathbf{r}) \;=\; \frac{W_0}{W(z)} \exp\left(\frac{-\rho^2}{W^2(z)}\right) \exp\left(ikz + ik\frac{\rho^2}{2R(z)} - i\zeta(z)\right), \tag{3}$$

where $\rho^2 = x^2 + y^2$, $k = nk_0$ is the wavenumber (n, the refractive index of the surrounding medium, which we assume non-absorptive, and $k_0 = \omega/c = 2\pi/\lambda$, the vacuum wavenumber), $W(z) = W_0\sqrt{1 + (z/z_0)^2}$ and $W_0 = \sqrt{\lambda z_0/n\pi}$ are the beam width and the waist radius (beam width at $z = 0$), respectively, z_0 is the Rayleigh range, $R(z) = z(1 + (z_0/z)^2)$ is the

radius of curvature of the beam's wavefronts and $\zeta(z) = \tan^{-1}(z/z_0)$ is the so-called Gouy phase at z. In the far field ($z \gg \lambda$, z_0), $W(z) \approx (W_0/z_0)z$, hence W_0 and z_0 can both be expressed in terms of the beam's numerical aperture ($\mathrm{NA}_b = n\sin\theta_0$, being θ_0 the beam's divergence angle) as $W_0 = \lambda/(\pi \mathrm{NA}_b)$ and $z_0 = \lambda n/(\pi(\mathrm{NA}_b)^2)$.

The origin of the coordinate system for our analysis is located at the focal region center and the propagating direction, coincident with optical axis, is fixed along the $\hat{z}$ direction in Equation (3). This reference system will be used throughout the paper. The Gaussian beam approximation fails for highly divergent beams; it is valid when wavefronts are tilted with respect to the optical axis less than a threshold angle θ_c such that $\sin\theta_c \approx \theta_c$ (paraxial approximation).[34] This condition is fulfilled for $\theta_0 \leq \theta_c \approx 30^\circ$ and we will show that yields effective optical confinement in three dimensions (3D) for NPs. To analyze the resulting optical forces and to provide equilibrium positions along the optical axis and stiffness constants in the three spatial directions, we next study a general NP, namely, a small object with both scattering and absorbing behaviors.

Optical forces on a small particle

The time-averaged force components on a subwavelength-sized particle in an arbitrary time-harmonic electromagnetic field is:[35]

$$\langle F_i(\mathbf{r})\rangle = \frac{1}{2}\Re e\left\{\alpha \mathbf{E}(\mathbf{r}) \cdot (\partial_i \mathbf{E}^*(\mathbf{r}))\right\}. \tag{4}$$

where $i = x, y, z$ are the Cartesian force components and ∂_i is the partial derivative with respect to the corresponding spatial coordinate. The optical behavior of the particle is described by the complex polarizability, α, which is a sufficient description provided that the particle can be approximated by a dipole. The total time-averaged force can be expressed as the sum of a gradient and an *extinction* force, the latter representing both the scattering

and absorption optical effects on the NP:

$$\left\langle \vec{F}(\mathbf{r}) \right\rangle = \left\langle \vec{F}(\mathbf{r}) \right\rangle_{gra} + \left\langle \vec{F}(\mathbf{r}) \right\rangle_{ext}. \tag{5}$$

Introducing the complex amplitude expressed in Equation (3) in Equation (2), and then in Equation (4), and separating for the real and imaginary parts for the polarizability to address the force components in Equation (5), we find the next results:

$$\langle F_x(\mathbf{r}) \rangle_{gra} = -\frac{1}{2} I(\mathbf{r}) \Re e \{\alpha\} \left(\frac{2x}{W^2(z)} g(\mathbf{r}) - \frac{|f_x|^2 x + \Re e \{f_x^* f_y\} y}{z^2 + z_0^2} \right), \tag{6}$$

$$\langle F_y(\mathbf{r}) \rangle_{gra} = -\frac{1}{2} I(\mathbf{r}) \Re e \{\alpha\} \left(\frac{2y}{W^2(z)} g(\mathbf{r}) - \frac{\Re e \left\{f_x f_y^*\right\} x + |f_y|^2 y}{z^2 + z_0^2} \right), \tag{7}$$

$$\langle F_z(\mathbf{r}) \rangle_{gra} = -\frac{1}{2} I(\mathbf{r}) \Re e \{\alpha\} \left[\frac{|f_x x + f_y y|^2}{\left(z^2 + z_0^2\right)^2} z + g(\mathbf{r}) \frac{z}{z_0^2} \left(\frac{W_0}{W(z)} \right)^2 \left(1 - \frac{2\rho^2}{W^2(z)} \right) \right]. \tag{8}$$

$$\langle F_x(\mathbf{r}) \rangle_{ext} = \frac{1}{2} I(\mathbf{r}) \Im m \{\alpha\} \left(\frac{kx}{R(z)} g(\mathbf{r}) - \frac{\Im m \{f_x^* f_y\} y}{z^2 + z_0^2} \right), \tag{9}$$

$$\langle F_y(\mathbf{r}) \rangle_{ext} = \frac{1}{2} I(\mathbf{r}) \Im m \{\alpha\} \left(\frac{ky}{R(z)} g(\mathbf{r}) - \frac{\Im m \left\{f_x f_y^*\right\} x}{z^2 + z_0^2} \right), \tag{10}$$

$$\langle F_z(\mathbf{r}) \rangle_{ext} = \frac{1}{2} I(\mathbf{r}) \Im m \{\alpha\} \left[\frac{|f_x x + f_y y|^2}{\left(z^2 + z_0^2\right)^2} z_0 + g(\mathbf{r}) \left(k \left(1 - \frac{\rho^2}{2} \frac{z^2 - z_0^2}{(z^2 + z_0^2)^2} \right) - \frac{1}{z_0} \left(\frac{W_0}{W(z)} \right)^2 \right) \right], \tag{11}$$

where

$$I(\mathbf{r}) = \frac{1}{p} I_0 |U(\mathbf{r})|^2, \;\; I_0 = |E_0|^2, \tag{12}$$

$$|U(\mathbf{r})|^2 = \left(\frac{W_0}{W(z)}\right)^2 \exp\left(-\frac{2\rho^2}{W^2(z)}\right), \tag{13}$$

$$g(\mathbf{r}) = p + \frac{|f_x x + f_y y|^2}{z^2 + z_0^2}. \tag{14}$$

The relation between the incident electric field, E_0, for a general polarization-state weakly-focused beam, Equation (2), and the resulting optical power is explained in the Supporting Information.

The fact that the terms that accompany the real part of the polarizability are gradient forces and those going with its imaginary part constitute the radiation pressure, as contributed by scattering and absorption light effects on the NP, was justified elsewhere for a general paraxial beam in the Rayleigh approximation ($ka \ll 1$, being a the radius of the NP).[36,37] Basically, the real part of the polarizability accompanies the gradient of the light beam intensity, whereas the imaginary part of the polarizability goes with the intensity in the expression of the total optical force on a NP under a paraxial light beam. The imaginary part of the polarizability is in turn proportional to the scattering and absorption cross sections for very small particles compared to the wavelength. The additional term in the equation of the total force, as obtained in,[36,37] which is also proportional to the imaginary part of the polarizability, was explained to be related to the spin angular momentum of the light field elsewhere.[38] The presence of this term manifests in our calculations through the fact that the force in the $\hat{x}$ direction, Equations (6) and (9), do not exhibit symmetry on interchanging $x \leftrightarrow y$ with the force in the $\hat{y}$ direction, Equations (7) and (10).

Analytical expressions to address the polarizability of general nanostructures, including coated NPs, within the dipolar approximation are described in the Supporting Information and Figure S4.

Equilibrium conditions and trapping stiffnesses

The condition for stability, $\langle F_i(\mathbf{r})\rangle = 0$, applied to the directions orthogonal to the optical axis is straightforward to examine, and yields $x_{eq} = y_{eq} = 0$. Axial stability then implies

$$\Re e\left\{\alpha\right\}\frac{z}{z_0}\left(\frac{W_0}{W(z)}\right)^2 = \Im m\left\{\alpha\right\}\left(kz_0 - \left(\frac{W_0}{W(z)}\right)^2\right). \tag{15}$$

The closer to the focal region center, the higher the probability of optical confinement. In practice, simple physical inspection of the axial stability involves that $z \ll z_0$. Applying this approximation to Equation (15), we obtain the equilibrium position in the optical axis:

$$\frac{z_{eq}}{z_0} = \frac{\Im m\left\{\alpha\right\}}{\Re e\left\{\alpha\right\}}\left(kz_0 - 1\right). \tag{16}$$

Linearization of Equation (5) (with gradient and extinction components given by Equations (6-11)) around $\mathbf{r}_{eq} = (0, 0, z_{eq})$ provides expressions for the spring constants in the three spatial directions:

$$\kappa_x = \kappa_y = \Re e\left\{\alpha\right\}\frac{I_0}{W_0^2}, \tag{17}$$

$$\kappa_z = \Re e\left\{\alpha\right\}\frac{1}{2}\frac{I_0}{z_0^2}; \tag{18}$$

these stiffnesses describe the optical trap near the focal region center according to a Hooke's law: $\langle F_i(i)\rangle = -\kappa_i i$, with $i = x, y, z$. Noticeably, trap physics near the center of the focal region does not depend on the optical absorption of the NP, as observed from the absence of the imaginary part of the polarizability in Equations (17-18). The ratio of stiffnesses yield:

$$\frac{\kappa_z}{\kappa_{x,y}} = \frac{1}{kz_0}, \tag{19}$$

implying that for weak focusing (long z_0), trapping efficiency is larger in the transversal directions and that the ratio between the transversal and the axial stiffnesses does not depend

on the optical power.

Experiment

We next evaluate experimentally the above theoretical results with iron oxide NPs of different compositions. These particles are within or slightly above the Rayleigh size range. The optical properties of magnetite (Fe_3O_4) NPs have been analyzed in several reports,[39–42] and experimental data for the dielectric constant are available.[43] Therefore, we can perform predictions with the above theoretical analysis and verify them experimentally.

Early reports on optical trapping of iron oxide NPs did not show 3D optical confinement by just a focused beam.[44–46] With the aim of understanding this problem and to yield net optical trapping stability, we synthesized two types of NPs (Methods and Supporting Information): an Fe_3O_4 (IONP) sample with mean diameter $2a = 11 \pm 1$ nm (Figure 1, (a) and (b)) and two samples of silica coated iron oxide NPs (IONP@SiO_2) with the next size distribution parameters: Type I: core diameter, $2a_c = 11 \pm 1$ nm; total diameter, $2a = 99 \pm 4$ nm (Figure 1, (c) and (d)). Type II: $2a_c = 22 \pm 3$ nm, $2a = 50 \pm 5$ nm (Figures S1 and S2). The magnetic characterizations of these samples are also explained in the Supporting Information, including Figure S3.

The description of our optical tweezers setup can be found in the Methods section. We used $\lambda = 808$ nm, $f_x = 1$ and $f_y = -i$ (circular polarization in the trap), $n = 1.333$ (water), $\mathrm{NA}_b \approx 0.5$ (NA = 1.2, water-immersion objective lens), which makes $\theta_0 = 22°$, within the paraxial approximation, and $2z_0 \approx 2740$ nm and $2W_0 \approx 1030$ nm for the axial and transversal dimensions, respectively, of the focal region in our optical trapping design.

We observed experimentally that IONPs and IONP@SiO_2 (type II) escape from the focal region along the beam's propagating direction. On the contrary, IONP@SiO_2 (type I) remained stable in the optical trap. The theoretical predictions are shown in Figure 3. It is observed that there is not net optical stability in 3D for the IONPs. The radiation pressure

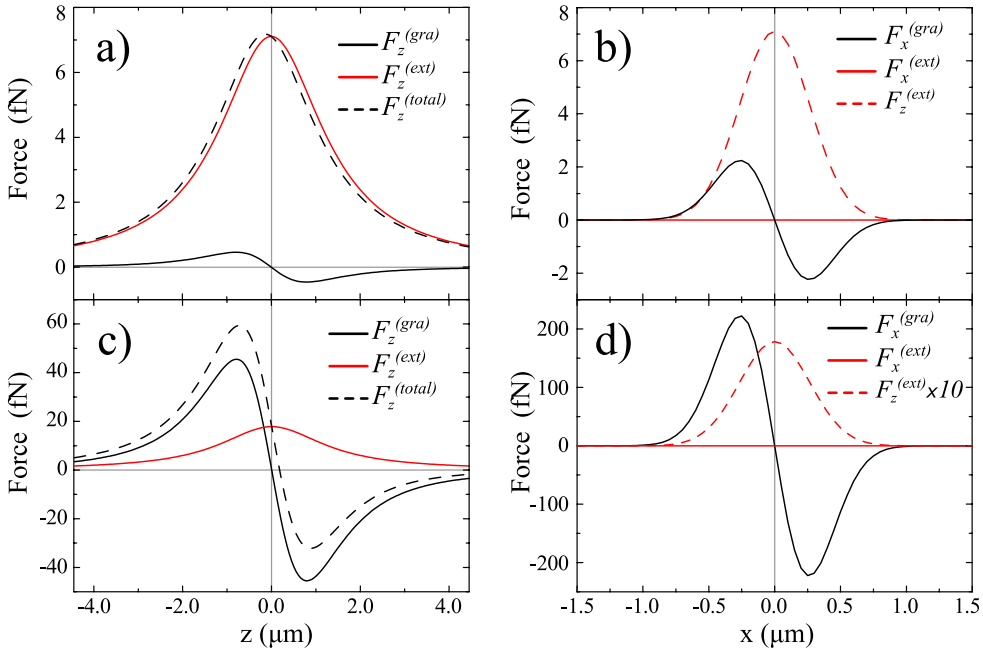

Figure 3: Average optical forces at the optical axis ($x = y = 0$), (a), and at the laser focus ($z = y = 0$), (b), for a single IONP. Analogue plots, (c) and (d), respectively, for an IONP@SiO_2 (type I). Laser power, 100 mW.

exerted in the axial direction, Figure 3(a), dominate the gradient force. Therefore, the particle escapes in the beam's propagating direction, despite there is optical stability in the transvesal directions, Figure 3(b). Similar qualitative results were obtained for IONP@SiO_2 (type II), see Figure S5 in the Supporting Information. Finally, IONP@SiO_2 (type I) particles can be trapped in 3D: there is optical stability both in the axial and transversal directions (Figure 3, (c) and (d), respectively). The addition of a transparent coating to the IONP cores increases refraction with respect to absorption, making gradient forces dominate the radiation pressure and hence yielding net optical confinement in 3D.[47]

To obtain a quantitative comparison between theory and experiment, we measure the spring constants in the transversal and axial directions for an IONP@SiO_2 (type I) in the optical trap. The power spectrum densities (PSDs) of the force fluctuations of an individual NP at two laser powers are plotted in Figure 4(a). Characteristic corner frequencies, f_c, were obtained from each PSD measurement (Methods and Figure 2). Corresponding drag

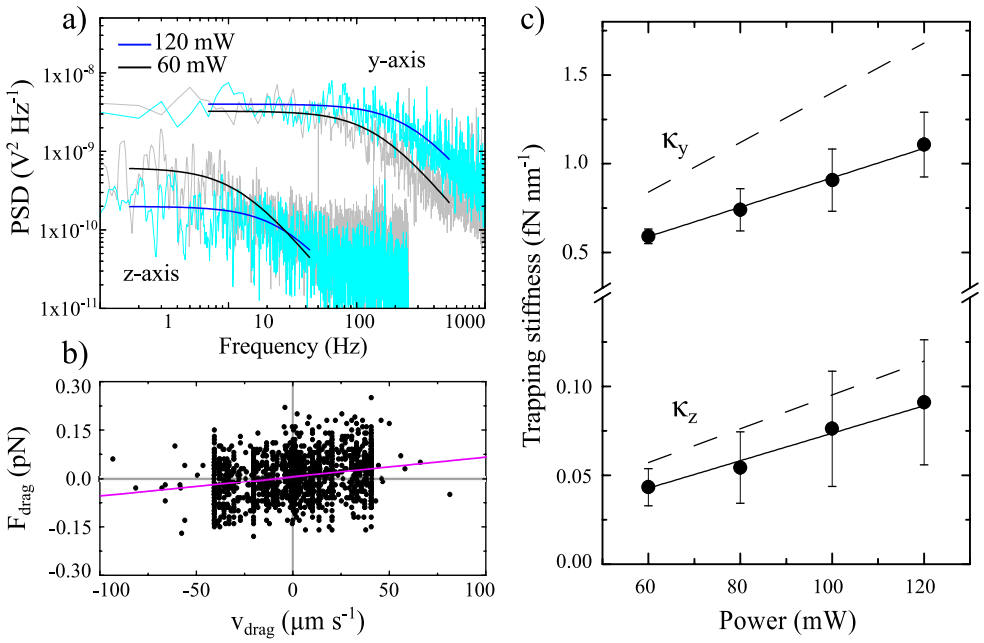

Figure 4: Experimental determination of the trapping stiffnesses of single nanoparticles. (a) Power spectrum densities (PSDs) of the force fluctuations of an IONP@SiO_2 (type I) at $P_{trap} = 120$ mW (blue) and $P_{trap} = 60$ mW (grey). Overlapped curves are Lorentzian fits to the experimental data, yielding corner frequencies of $f_c = 262 \pm 7$ Hz and $f_c = 143 \pm 8$ Hz for y-axis fluctuations and $f_c = 17.4 \pm 5.0$ Hz and $f_c = 10.2 \pm 0.5$ Hz for z-axis ($P_{trap} = 120$ mW, dark blue curve, and $P_{trap} = 60$ mW, black curve, respectively). For z-axis, PSDs were deliberately truncated below Nyquist frequency for the sake of clarity. (b) Stokes' law test of an IONP@SiO_2 (type I) at $P_{trap} = 120$ mW along the y-axis. Best fitting line to $F_{drag} = \gamma v_{drag}$ yields a drag coefficient of $\gamma = (6.0 \pm 0.3) \times 10^{-4}$ pN s μm^{-1}. (c) Average (mean $\pm$ SD) lateral (κ_y) and axial (κ_z) trapping stiffnesses calculated from the corner frequency and the drag coefficient measurements for five individual IONP@SiO_2 (type I) sample NPs. Solid lines are the best linear fit to experimental data, whereas dash lines are the theoretical predictions.

coefficients, γ, were measured from the Stokes' law (Methods), as shown in Figure 4(b). These data are directly taken in our optical setup since it is calibrated by using the linear momentum conservation principle (Methods). The trapping stiffnesses were derived as $\kappa = 2\pi f_c \gamma$. Concurrent determination of γ and f_c for each NP in the trap avoids the use of hypotheses on actual size, geometry or composition of the specific NP in the trap or the viscosity of the medium, which may change as a result of mild optical heating from the NP. Figure 4(c) shows the trap stiffnesses vs. optical power at the focal region in the

transversal and axial directions, along with the theoretical predictions. The amplitude of the force fluctuations in the transversal directions, $\hat{x}$ and $\hat{y}$, were similar (Figure 2), confirming trapping homogeneity in this plane.

Calculations at 100 mW using Equation (17) yield $\kappa_x = \kappa_y = 1.45$ pN/μm, very closed to the numerical prediction (i.e. $\kappa_i = \partial_i F_i|_{(x_{eq},y_{eq},z_{eq})}$ where $i = x, y, z$), $\kappa_x = \kappa_y = 1.40$ pN/μm, hence confirming the validity of the approximations above. Experimentally, $\kappa_y = 0.91 \pm 0.09$ pN/μm for the sample NP shown in Figure 4(c). In these conditions, according to Equation (16), the theoretical position for this type of NP in the trap is $z_{eq} = 174.5$ nm (177.6 nm by solving $F_z(z_{eq}) = 0$ numerically), with $x_{eq} = y_{eq} = 0$. With regards to the trapping stiffness along the optical axis, the theoretical prediction at 100 mW is $\kappa_z = 0.102$ pN/μm (0.0953 pN/μm numerically), whereas the experimental measurement yielded $\kappa_z = 0.07 \pm 0.03$ pN/μm for the sample NP shown in Figure 4(c). κ_z is about ten times smaller than κ_x and κ_y, as confirmed by the theoretical prediction, Equation (19): $\kappa_z/\kappa_{x,y} = 0.070$ (0.068 numerically and 0.08 ± 0.01 experimentally), in agreement with results for much tighter traps.[20]

The force components for $y = x = 0$, $\langle F_x(z)\rangle_{gra} = \langle F_x(z)\rangle_{ext} = 0$ and $\langle F_y(z)\rangle_{gra} = \langle F_y(z)\rangle_{ext} = 0$ for all the NPs. Similarly, the force components $\langle F_x(0,y,0)\rangle_{gra} = 0$ and $\langle F_y(x,0,0)\rangle_{gra} = 0$. However, the force components $\langle F_x(0,y,0)\rangle_{ext}$ and $\langle F_y(x,0,0)\rangle_{ext}$, though very small, are not negligible. In fact, these force components generate an optical torque to the NP in the trap, as shown in Figure 5 for the IONP@SiO_2 (type I) sample NPs. The top panel of this figure is a vector field plot exhibiting the resulting optical vortex, whereas the bottom panel shows the magnitude of the torque-generating forces, which is four orders of magnitude smaller than the trapping forces (see Figure 3(c)).

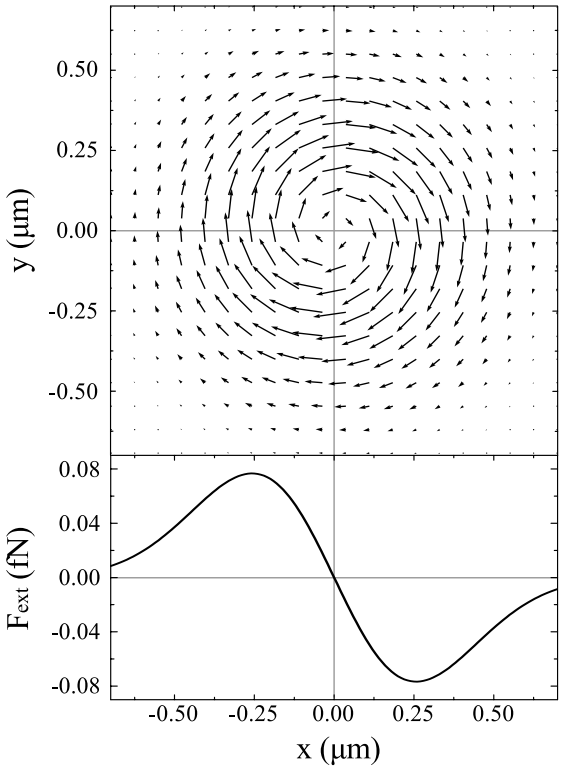

Figure 5: Average torque at the laser focus for a single, optically-trapped IONP@SiO2 (type I). Top panel, lateral optical extinction force field at $z = 0$. Bottom panel, magnitude of $\langle F_y(x, 0, 0)\rangle_{ext}$. The corresponding plot for $\langle F_x(0, y, 0)\rangle_{ext}$ has opposite sign in the vertical axis. Laser power, 100 mW.

Discussion

The comparison between experiments and theory exhibits good agreement. On one hand, the qualitative behavior of the NPs, namely, the trapping effectiveness, is rigorously predicted by the theory. On the other hand, having in mind the size dispersion in the NP preparation, not mentioning geometrical deffects or composition transitions between magnetite and maghemite, the quantitative agreement is quite reasonable.

Based on this consistency, we now discuss the influence of the beam numerical aperture and core and shell sizes in the optical trapping. As detailed in the Supporting Information, for the former, stable optical trapping is not possible for single IONP@SiO_2 (type I) NPs below $NA_b \approx 0.35$ (Figure S6). For the latter (Figure S7), silica encapsulation only enables

the trapping of Fe_3O_4 cores with radius smaller than $a_c = 10$ nm, provided that silica shells remain in the range 30 nm $< a <$ 90 nm, using beams with NA_b=0.5. These predictions arise not only due to the fact that gradient forces may not counterbalance the extinction effects outside these ranges but also due to the magnitude of the forces, which may be too low (on the order of 1 fN in theoretically limiting conditions) to hold a NP in the presence of noise.

The dielectric constants for the magnetite were obtained from bulk experiments, in which the material had macroscopic dimensions.[43] In this regard, we have discarded magnetic effects at optical frequencies for the iron oxide NPs (namely, deviations from the supposed relative magnetic susceptibility $\mu_r = 1$). Since a magnetodielectric behavior has been described for magnetite,[48] including effects at optical frequencies,[49] we have performed a rigorous theoretical analysis of these effects[50–54] in the experimental conditions described above (Supporting Information). We have found a very low contribution of the first magnetic Mie coefficient for the Fe_3O_4@SiO_2 NPs and a negligible effect for the Fe_3O_4 NPs with respect to the first electric Mie coefficient.[55,56] Likewise, in order to assess the validity of the dipolar approximation, we have evaluated the second electric and magnetic Mie coefficients[55,56] finding that their contributions are also very small. Both sets of numerical results confirm the validity of our theoretical analysis above.

Due to the low trapping forces that may experience very small particles, thermal fluctuations at ambient temperature in liquid media may in practice prevent optical trapping. However, due to the high dynamical stability of our tweezers setup, this did not happen in our assays and trapping forces as low as of some tens of fN were sufficient to maintain a stable confinement of the NPs in the trap (for minutes).

Conclusions

We have demonstrated optical trapping of single NPs in weakly-focused beams and have revealed the stringent theoretical conditions that are required. We show that the effectiveness of optical trapping depends on the material properties of the NP through the polarizability and that stiffnesses of the trap in the three spatial directions only depend on the refractive properties of the NP. The transversal stiffnesses are around ten times larger than the axial stiffness and the region visited by the confined NP can be assimilated as an ellipsoid with long axis in the beam's propagating direction and typical dimensions of a few micrometers.

Optical manipulation is therefore possible in conditions in which radiation damage has to be reduced.

Our theoretical results are analytical, thus making possible to predict effective optical trapping without the need of experimental tests or the burden of cumbersome numerical computations.

Finally, we have demonstrated optical control of iron oxide NPs, for which, due to the importance of energy losses, 3D confinement had not been possible to date. We have made it possible through a chemical strategy: by using a silica coating, which makes the effective behavior of the NP in the optical field approach a purely transparent NP. This strategy increases the magnitude of the gradient forces, ultimately responsible for the optical trapping.

Acknowledgement

We are grateful to Dr. María Acebrón and Dr. Beatriz H. Juárez for their support in the silica encapsulation of the nanoparticles. This work was supported by the Spanish Ministry of Economy and Competitiveness (MINECO, Grant MAT2015-71806-R). IMDEA Nanociencia acknowledges support from the 'Severo Ochoa' Programme for Centers of Excellence in R&D (MINECO, Grant SEV-2016-0686). H.R-R. is supported by an FPI-UAM fellowship.

Supporting Information Available

The following files are available free of charge.

- Additional information on the synthesis of the nanoparticles, power and electric field at the optical trap center, polarizability, prediction on optical trapping of iron oxide nanoparticles coated by silica with bigger iron oxide core and smaller silica mantle (IONP@SiO_2 (type II)), limits for the optical stability of core-shell iron-oxide nanoparticles, magnetic response of Fe_3O_4 at optical frequencies and validity of the dipolar approximation.

References

(1) Lehmuskero, A.; Johansson, P.; Rubinsztein-Dunlop, H.; Tong, L.; Käll, M. Laser trapping of colloidal metal nanoparticles. *ACS Nano* **2015**, *9*, 3453–3469.

(2) Heller, I.; Hoekstra, T. P.; King, G. A.; Peterman, E. J. G.; Wuite, G. J. L. Optical tweezers snalysis of DNA-protein complexes. *Chem. Rev.* **2014**, *114*, 3087–3119.

(3) Arias-Gonzalez, J. R. Single-molecule portrait of DNA and RNA double helices. *Integr. Biol.* **2014**, *6*, 904–925.

(4) Marago, O. M.; Jones, P. H.; Gucciardi, P. G.; Volpe, G.; Ferrari, A. C. Optical trapping and manipulation of nanostructures. *Nat. Nanotech.* **2013**, *8*, 807–819.

(5) Usman, A.; Chiang, W.-Y.; Masuhara, H. Optical trapping of nanoparticles by ultrashort laser pulses. *Sci. Prog.* **2013**, *96*, 1–18.

(6) Arias-Gonzalez, J. R. Optical tweezers to study viruses. *Subcell. Biochem.* **2013**, *68*, 273–304.

(7) Dienerowitz, M.; Mazilu, M.; Dholakia, K. Optical manipulation of nanoparticles: a review. *J. Nanophotonics* **2008**, *2*, 021875–021875.

(8) Ashkin, A.; Dziedzic, J. M.; Biorkholm, J. E.; Chu, S. Observation of a single-beam gradient force optical trap for dielectric particles. *Opt. Lett.* **1986**, 288–290.

(9) Hormeño, S.; Arias-Gonzalez, J. R. Exploring mechanochemical processes in the cell with optical tweezers. *Biol. Cell* **2006**, *98*, 679–695.

(10) Schmidt, F.; Magazzù, A.; Callegari, A.; Biancofiore, L.; Cichos, F.; Volpe, G. Microscopic engine powered by critical demixing. *Phys. Rev. Lett.* **2018**, *120*, 068004.

(11) Rodríguez-Rodríguez, H.; Acebrón, M.; Juárez, B. H.; Arias-Gonzalez, J. R. Luminescence dynamics of silica-encapsulated quantum dots during optical trapping. *J. Phys. Chem. C* **2017**, *121*, 10124–10130.

(12) Nørregaard, K.; Ralf, M.; Ritter, C. M.; Berg-Sørensen, K.; Oddershede, L. B. Manipulation and motion of organelles and single molecules in living cells. *Chem. Rev.* **2017**, acs.chemrev.6b00638.

(13) Montange, R. K.; Bull, S. M.; Shanblatt, E. R.; Perkins, T. T. Optimizing bead size reduces errors in force measurements in optical traps. *Opt. Express* **2013**, *21*, 39–48.

(14) Balijepalli, A.; Gorman, J. J.; Gupta, S. K.; LeBrun, T. W. Significantly improved trapping lifetime of nanoparticles in an optical trap using feedback control. *Nano Lett.* **2012**, *12*, 2347–2351.

(15) Iglesias, I.; Saenz, J. J. Scattering forces in the focal volume of high numerical aperture microscope objectives. *Opt. Commun.* **2011**, *284*, 2430–2436.

(16) XiaoYu, L.; Feng, W. Influence of the laser parameters on trapping gold nanoparticles. 2010 Academic Symposium on Optoelectronics and Microelectronics Technology and 10th Chinese-Russian Symposium on Laser Physics and Laser TechnologyOptoelectronics Technology (ASOT). 2010; pp 192–195.

(17) Jauffred, L.; Oddershede, L. B. Two-photon quantum dot excitation during optical trapping. *Nano Lett.* **2010**, *10*, 1927–1930.

(18) Bosanac, L.; Aabo, T.; Bendix, P. M.; Oddershede, L. B. Efficient optical trapping and visualization of silver nanoparticles. *Nano Lett.* **2008**, *8*, 1486–1491.

(19) Hansen, P. M.; Bhatia, V. K.; Harrit, N.; Oddershede, L. B. Expanding the optical trapping range of gold nanoparticles. *Nano Lett.* **2005**, *5*, 1937–1942.

(20) Rohrbach, A. Stiffness of optical traps: Quantitative agreement between experiment and electromagnetic theory. *Phys. Rev. Lett.* **2005**, *95*, 1–4.

(21) Brzobohatý, O.; Šiler, M.; Trojek, J.; Chvátal, L.; Karásek, V.; Paták, A.; Zuzana, P.; Mika, F.; Zemánek, P. Three-dimensional optical trapping of a plasmonic nanoparticle using low numerical aperture optical tweezers. *Sci. Rep.* **2015**, *5*, 8106.

(22) Hormeño, S.; Gregorio-Godoy, P.; Perez-Juste, J.; Liz-Marzan, L. M.; Juarez, B. H.; Arias-Gonzalez, J. R. Laser heating tunability by off-resonant irradiation of gold nanoparticles. *Small* **2014**, *10*, 376–384.

(23) Hormeño, S.; Ibarra, B.; Chichón, F. J.; Habermann, K.; Lange, B. M. H.; Valpuesta, J. M.; Carrascosa, J. L.; Arias-Gonzalez, J. R. Single centrosome manipulation reveals its electric charge and associated dynamic structure. *Biophys. J.* **2009**, *97*, 1022–1030.

(24) Smith, S. B.; Cui, Y.; Bustamante, C. Optical-trap force transducer that operates by direct measurement of light momentum. *Methods Enzymol.* **2003**, *361*, 134–162.

(25) Farre, A.; Montes-Usategui, M. A force detection technique for single-beam optical traps based on direct measurement of light momentum changes. *Opt. Express* **2010**, *18*, 11955–11968.

(26) Vermeulen, K. C.; Wuite, G. J. L.; Stienen, G. J. M.; Schmidt, C. F. Optical trap stiffness in the presence and absence of spherical aberrations. *Appl. Opt.* **2006**, *45*, 1812–1819.

(27) Ortega, D.; Pankhurst, Q. A. In *Nanoscience, Vol 1: Nanostructures through Chemistry*; Obrien, P., Ed.; 2013; Vol. 1; pp 60–88.

(28) Espinosa, A.; Di Corato, R.; Kolosnjaj-Tabi, J.; Flaud, P.; Pellegrino, T.; Wilhelm, C. Duality of iron oxide nanoparticles in cancer therapy: amplification of heating efficiency by magnetic hyperthermia and photothermal bimodal treatment. *ACS Nano* **2016**, *10*, 2436–2446.

(29) Yuan, G.; Yuan, Y.; Xu, K.; Luo, Q. Biocompatible PEGylated Fe_3O_4 nanoparticles as photothermal agents for near-infrared light modulated cancer therapy. *Int. J. Mol. Sci.* **2014**, *15*, 18776–18788.

(30) Chu, M.; Shao, Y.; Peng, J.; Dai, X.; Li, H.; Wu, Q.; Shi, D. Near-infrared laser light mediated cancer therapy by photothermal effect of Fe_3O_4 magnetic nanoparticles. *Biomaterials* **2013**, *34*, 4078–4088.

(31) Khosroshahi, M. E.; Ghazanfari, L.; Hasan-Nejad, Z. Preliminary results of treating cancerous cells of lung (QU-DB) by hyperthermia using diode laser and gold coated Fe_3O_4/SiO2 nano-shells: an in-vitro assay. *Iran J. Med. Phys.* **2012**, *9*, 253–263.

(32) Andrë, W.; D'Ambly, C. G.; Hergt, R.; Hilger, I.; Kaiser, W. A. Temperature distribution as function of time around a small spherical heat source of local magnetic hyperthermia. *J. Magn. Magn. Mater.* **1999**, *194*, 197–203.

(33) de Lorenzo, S.; Ribezzi-Crivellari, M.; Arias-Gonzalez, J. R.; Smith, S. B.; Ritort, F. A temperature-jump optical trap for single-molecule manipulation. *Biophys. J.* **2015**, *108*, 2854–2864.

(34) Saleh, B. E. A.; Teich, M. C. *Fundamentals of photonics*; 2001.

(35) Chaumet, P. C.; Nieto-Vesperinas, M. Time-averaged total force on a dipolar sphere in an electromagnetic field. *Opt. Lett.* **2000**, *25*, 1065–1067.

(36) Arias-Gonzalez, J. R.; Nieto-Vesperinas, M. Optical forces on small particles: attractive and repulsive nature and plasmon-resonance conditions. *J. Opt. Soc. Am. A Opt. Image Sci. Vis.* **2003**, *20*, 1201–1209.

(37) Nieto-Vesperinas, M.; Arias-González, J. R. Theory of forces induced by evanescent fields. *arXiv* **2011**, 1102.1613 [cond–mat.other].

(38) Albaladejo, S.; Marques, M. I.; Laroche, M.; Saenz, J. J. Scattering forces from the curl of the spin angular momentum of a light field. *Phys. Rev. Lett.* **2009**, *102*, 113602.

(39) Sadat, M. E. Photoluminescence and photothermal effect of Fe_3O_4 nanoparticles for medical imaging and therapy. *Appl. Phys. Lett.* **2014**, *105*, 91903.

(40) Milichko, V.; Nechaev, A. I.; Valtsifer, V.; Strelnikov, V. N.; Kulchin, Y. N.; Dzyuba, V. P. Photo-induced electric polarizability of Fe_3O_4 nanoparticles in weak optical fields. *Nanoscale Res. Lett.* **2013**, *8*, 317.

(41) Tang, J.; Myers, M.; Bosnick, K. a.; Brus, L. E. Magnetite Fe_3O_4 nanocrystals : Spectroscopic observation of aqueous oxidation kinetics. *J. Phys. Chem. B* **2003**, *107*, 7501–7506.

(42) Rossman, G. R. In *Mineral Spectroscopy; A Tribute to Roger G. Burns*, special publication no. 5, 1996 ed.; Dyar, M., McCammon, C., Schaefer, M., Eds.; 1996; pp 23–27.

(43) Schlegel, A.; Alvarado, S. F.; Wachter, P. Optical properties of magnetite (Fe_3O_4). *J. Phys. C-Solid State Physics* **1979**, *12*, 1157–1164.

(44) Meng, Z.-M.; Liu, H.-Y.; Zhao, W.-R.; Zhang, W.; Deng, H.-D.; Dai, Q.-F.; Wu, L.-J.; Lan, S.; Gopal, A. V. Effects of optical forces on the transmission of magnetic fluids investigated by Z-scan technique. *J. Appl. Phys.* **2009**, *106*, 044905.

(45) Deng, H.; Zhang, C.; Yang, X.; Guo, Z.; Zhou, W. Two-dimensional optical trapping and clustering of magnetic nanoparticles. *Sci. Sin-Phys. Mech. Astron.* **2014**, *44*, 557.

(46) Xu, H.; Jones, S.; Choi, B.-C.; Gordon, R. Characterization of individual magnetic nanoparticles in solution by double nanohole optical tweezers. *Nano Lett.* **2016**, *16*, 2639–2643.

(47) Spadaro, D.; Iatì, M. A.; Donato, M. G.; Gucciardi, P. G.; Saija, R.; Cherlakola, A. R.; Scaramuzza, S.; Amendola, V.; Maragò, O. M. Scaling of optical forces on Au-PEG core-shell nanoparticles. *RSC Adv.* **2015**, *5*, 93139.

(48) Chang, C.-C.; Zhao, L.; Wu, M.-K. Magnetodielectric study in SiO_2-coated Fe_3O_4 nanoparticle compacts. *J. Appl. Phys.* **2010**, *108*.

(49) Caicedo, J. M.; Arora, S. K.; Ramos, R.; Shvets, I. V.; Fontcuberta, J.; Herranz, G. Large magnetorefractive effect in magnetite. *New J. Phys.* **2010**, *12*, 1–8.

(50) Arias-Gonzalez, J. R.; Nieto-Vesperinas, M. Near-field distributions of resonant modes in small dielectric objects on flat surfaces. *Opt. Lett.* **2000**, *25*, 782–784.

(51) Arias-Gonzalez, J. R.; Nieto-Vesperinas, M. Resonant near-field eigenmodes of nanocylinders on flat surfaces under both homogeneous and inhomogeneous lightwave excitation. *J. Opt. Soc. Am. A Opt. Image Sci. Vis.* **2001**, *18*, 657–665.

(52) Garcia-Etxarri, A.; Gomez-Medina, R.; Froufe-Perez, L. S.; Lopez, C.; Chantada, L.; Scheffold, F.; Aizpurua, J.; Nieto-Vesperinas, M.; Saenz, J. J. Strong magnetic response of submicron Silicon particles in the infrared. *Opt. Express* **2011**, *19*, 4815–4826.

(53) Nieto-Vesperinas, M.; Sáenz, J. J.; Gómez-Medina, R.; Chantada, L. Optical forces on small magnetodielectric particles. *Opt. Express* **2010**, *18*, 11428–11443.

(54) Chaumet, P. C.; Rahmani, A. Electromagnetic force and torque on magnetic and negative-index scatterers. *Opt. Express* **2009**, *17*, 2224–2234.

(55) Hulst, H. C.; van de Hulst, H. C. *Light scattering by small particles*; Dover Books on Physics; Dover Publications, 1957.

(56) Bohren, C. F.; Huffman, D. R. In *Absorption and scattering of light*; Publication, W.-I., Ed.; 1983.

TOC Graphic